20122400 3A

厚生労働科学研究費補助金

障害者対策総合研究事業(身体・知的等障害分野)

体幹保持機能障害のある身体障害者に対して生体内3次元解析システムを用いた脊椎骨構築
および動態情報フィードバック型革新的体幹保持デバイスの開発に関する研究

平成２４年度　総括・分担研究報告書

研究代表者　菅本　一臣

平成25(2013)年　5月

目　　次

厚生労働科学研究費補助金（障害者対策総合研究事業（身体・知的等障害分野））
統括研究報告書

体幹保持機能障害のある身体障害者に対して生体内3次元解析システムを用いた脊椎骨構築および動態情報フィードバック型革新的体幹保持デバイスの開発に関する研究

総括研究者 菅本 一臣 大阪大学大学院医学系研究科寄附講座教授

研究要旨　ポリカーボネイト製で作成した体幹デバイスの装着前後でコンピュータソフトを用いた評価システムを用いて、側弯における脊椎変形の3次元変形評価を行い。その矯正率を詳細に評価し、その最適装具作成条件を検討した。

梶浦一郎・社会福祉法人 愛徳福祉会 南大阪療育園 理事長
山崎隆治・大阪大学臨床医工学融合研究教育センター 特任准教授

A．研究目的

身体障害者に生じる体幹保持機能低下によって発症する側湾に対してポリカーボネイト製のカスタム体幹装具を作成する。その前後で脊椎変形の3次元変形評価を行い、最適の装具の作成を目指す。

B．研究方法

骨関節の構築を3次元的に解析できるシステムを開発してきたが、それを用いることにより骨関節形態を3次元的に評価することができる。今回脊椎側弯を有する身体障害者に対してポリカーボネイト製カスタム装具装着の前後でCTにて頚椎より骨盤にかけて撮影を行い、その矯正率を算出し、最適な装具開発を目指す。

（倫理面への配慮）

本研究は大学の倫理委員会にてすでに承認済みである。ただし被爆はゼロではなく、治療効果を正確に判定する目的があるとはいえ被験者に危険を及ぼす可能性があるために、インフォームドコンセントを得る必要がある。また得られたデータは個人情報として扱われるべきものであるため、そのデータ管理にはセキュリティーを十分考量する。

C．研究結果

脳性麻痺側彎症25例，特発性側彎症8例を対象とした．これを撮影したものを共同研究者の梶浦らに解析を行わせた。 その結果、Cobb角度で38度から22度へ約40％の改善率がみられた。

D．考察

これまで考えられてきた以上に側弯における脊椎変形は平面的なものではなく、3次元的な変形が大きく、それを今回提案したシステムで評価することによって、最適の装具を提供できた。

E．結論

本研究では，側彎における脊柱変形を3次元形態学的について明らかにした．特に回旋変形の評価はこれによって評価が可能であり、提案のポリカーボネイト製デバイスで 40％の改善が得られていることが明らかとなった。

F．健康危険情報

CTでは被爆量を通常の1/10以下でも可能であり、全脊椎を撮影しても5 mSv程度である。またそれは大学の倫理委員会にてすでに承認済みである。ただし被爆はゼロではなく、治療効果を正確に判定する目的があるとはいえ被験者に危険を及ぼす可能性があるために、インフォームドコンセントを得る必要がある。

G．研究発表

1.　論文発表

・Three-dimensional motion of the uncovertebral joint during head rotation. Nagamoto Y,Ishii T, Iwasaki M, Sakaura H, Moritomo H, Fujimori T, Kashii M, Murase T, Yoshikawa H, Sugamoto K. J Neurosurg Spine 2012 Oct;17(4):327-33.

・Kinematics of the thoracic spine in trunk rotation: in vivo 3-dimensional analysis. Fujimori T, Iwasaki M, Nagamoto Y, Ishii T, Kashii M, Murase T, Sugiura T, Matsuo Y, Sugamoto K, Yoshikawa H.Spine (Phila Pa 1976). 2012 Oct 1;37(21) E1318-28

・Three-dimensional measurement of intervertebral range of motion in ossification of the posterior longitudinal ligament: are there mobile segments in the continuous type? Fujimori T, Iwasaki M, Nagamoto Y, Kashii M, Ishii T, Sakaura H, Sugamoto K, Yoshikawa H. J Neurosurg Spine. 2012 Jul;17(1):74-81.

2.　学会発表

・Cervical Spine Research Society Asia Pacific region Apr. Japan Three-Dimensional Measurement of Intervertebral Range of Motion in Ossification of the Posterior Longitudinal Ligament Fujimori T, Iwasaki M, Nagamoto Y, Kashii M, Ishii T, Sakaura H, Sugamoto K, Yoshikawa H

・American Society of Biomechanics Aug. Florida In vivo three-dimensional analysis of the thoracic spine in trunk rotation Fujimori T Iwasaki M Nagamoto Y,Ishii T, Kashii M,Murase T, Sugamoto K, Yoshikawa H

H．知的財産権の出願・登録状況

1. 特許取得
特願2007－328479
2. 実用新案登録
なし
3. その他
なし

厚生労働科学研究費補助金（障害者対策総合研究事業（身体・知的等障害分野））
分担研究報告書

脳性麻痺側彎症における体幹保持破綻に伴う脊椎変形の生体内３次元解析に関する研究

研究分担者 梶浦　一郎　社会福祉法人大阪発達総合療育センター南大阪療育園理事長

研究要旨　肢体不自由児に代表されるような身体障害者において、体幹保持機能はADL上最も重要な機能のひとつである。本研究では体幹保持機能障害を有する身体障害者に対して革新的体幹保持デバイスの開発し、ADLを向上と続発する側弯などの不可逆的な脊椎変形を予防することを目的とする。また我々が開発してきた独自のシステムによりX線イメージ装置とCT装置を組み合わせて骨関節形態および動態を３次元的に解析し、身体特性データをフィードバックしながらデバイスを最適化する。

A．研究目的

身体障害者のADL上重要な体幹保持機能障害に対して、独自の３次元的解析を用いて骨関節形態および動態をフィードバックした革新的体幹保持デバイスを開発および最適化し、不可逆的な脊椎変形や生活機能の低下を予防する。

B．研究方法

対象は側弯を有する脳性麻痺患者150名（男性85名、女性65名）。平均年齢は14.7才。全脊椎2方向X線検査およびCTによりデバイス装着前後の側彎変形を評価した。デバイスによるADL変化について介護者アンケートを使用した。

(倫理面への配慮) CTは被爆量を通常の1/10以下、全脊椎撮影で５mSv程度である。またそれは大学の倫理委員会にてすでに承認済みである。撮影では被験者に危険を及ぼす可能性があるために、インフォームドコンセントを得る必要がある。リスクなどを口頭で説明し同意書に署名された場合のみ解析を行う。同意が得られなかった場合にはCT撮影は行わない。また得られたデータは個人情報として管理にはセキュリティーを十分考慮する。

C．研究結果

デバイスによる側彎矯正は平均17.9度、装着時間は8.1時間、治療中止は7例であった。CT解析ではHarrington Factorが低い（緩やかな）側彎変形ほど良好な矯正を得た。頂椎レベルと支柱形状は装着コンプライアンスに相関した。座位機能の安定、上肢機能の改善について再現性を認めた。

D．考察

側彎変形の形状に応じた支柱形状の決定によりCP患者の身体特性が反映され、高い矯正力と良好なコンプライアンスのデバイスが作成可能であった。継続的な装着によりADLの改善を認めた。

E．結論

当該デバイスの最適化により、側彎変形の矯正とADLの改善を認め、高いコンプライアンスを示した。CTによる３次元解析は身体特性フィードバックとデバイスの最適化に極めて有用であった。

G．研究発表

1.　論文発表
該当なし

2.　学会発表
・乳幼児期発症の側彎症に対する新しい装具治療の試み　第23回小児整形外科学会　2012年11月

・A novel spinal brace in management of scoliosis due to cerebral palsy. 国際整形外科学会(SICOT)　2012年11月

・Rett症候群に伴う側彎変形に対する装具(DSB)治療経過 第46回日本側彎症学会年次総会　2012年10月

・Management of scoliosis due to Rett syndrome with the novel spinal brace. ヨーロッパ神経学会(EFNS)　2012年9月

H．知的財産権の出願・登録状況

1.　特許取得
平成23年5月　「動的脊椎装具・プレーリーくん」特許取得　特許番号4747327

2.　実用新案登録
なし

3. その他
なし

厚生労働科学研究費補助金（障害者対策総合研究事業（身体・知的等障害分野））
分担研究報告書

X線透視画像を用いた骨関節３次元動態計測・解析の自動化に関する研究

研究分担者　山崎　隆治　大阪大学臨床医工学融合研究教育センター・特任准教授

研究要旨　平成22，23年度では，まず医用画像を用いた腰椎に特化した新しい３次元動態計測手法を開発し，変形腰椎を想定した検証実験を実施，最終的に各種椎骨（頸椎など）を含めた全椎骨の動態機能評価が可能な計測システムに拡張した．本研究（平成24年度）では，対象モデル（各種椎骨）の増加に伴う，計測・解析の多大な労力を軽減し，円滑に３次元動態計測・解析が可能なシステムの開発を試みた．本研究により，脊椎のような多数の骨で構成されるモデルにおいても，自動的に動態情報を計測・解析し，個々の症例に対応した動態情報フィードバック型の新しい体幹保持デバイスをスムーズに開発できる可能性が開けた．

A．研究目的

これまでの研究では，まずX線透視画像をベースとした腰椎に特化した新しい３次元動態計測手法を開発し，変形腰椎を想定した検証実験を実施，最終的に各種椎骨（頸椎など）を含めた全椎骨の動態機能評価が可能な計測システムを開発してきた．一方で，この計測システムでは，脊椎のような多数の骨で構成されるモデルを対象とした場合，種々の画像処理・画像解析過程で膨大なマニュアル作業が必要となり，円滑な３次元動態計測・解析を行う上で大きな障害となっていた．そこで本研究では，自動解析の妨げとなっていた画像の位置合わせ（レジストレーション）の際の対象モデルの初期点（適切な位置と姿勢の付与）の問題に着目し，３次元的な位置・姿勢が全てのX線フレームにわって自動的に，かつ安定に推定可能なシステムの開発を試みた．

B．研究方法

これまでの手法では，X線画像上の輪郭情報に起因する投影線とモデル表面上との距離値を評価関数とした，２次元/３次元画像位置合わせ技術（画像認識技術）を用いてきた．提案手法では，これまで動態解析を行った症例により作成される対象モデルの統計動態モデルを評価値として導入することにより，自動かつ安定した位置・姿勢推定を試みた．

実画像を用いた実験として，これまで人工膝関節を対象として動態解析データが多数蓄積されていることから（脊椎の解析データは，対象モデル数が多く膨大な時間がかかり，多数のデータが得られていないため），人工膝関節の統計動態モデルを作成，評価関数に導入し，提案手法による計測システムの性能評価を行った．このとき統計動態モデルとしては，対象モデル間の相対的な動態モデル（平均と分散）を利用した．

C．研究結果（実験および結果）

実際の人工膝関節屈曲動作におけるX線透視画像20症例を用いて，大腿骨・脛骨間の相対動作モデルをLeave-one-out法で作成し，実験を行った．

提案手法により，初期フレームを除き，全自動で（途中で破綻することなく）人工膝関節の位置・姿勢推定が可能なことが確認できた．また，その際の正解位置との距離誤差と角度誤差を算出した結果，0.63mm/1.46°であった．

D．考察

本研究における人工膝関節を対象とした３次元動態計測手法は，必要最小限のマニュアル作業で高精度な位置・姿勢推定結果が得られ，かつ安定であったことから，動態解析の自動化に有効であることが確認された．

E．結論

本研究の成果により，脊椎のような多数の骨で構成されるモデルに応用した場合も，自動的に動態情報を計測・解析し，個々の症例に対応した動態情報フィードバック型の新しい体幹保持デバイスをスムーズに開発できる可能性が開けた．

G．研究発表

1．論文発表

・3D Spine Kinematics on Riding Fitness Machines Using 2D/3D Image Registration, IFMBE Proceedings, Vol. 39, pp. 222-225, 2012

2．学会発表

・Initial pose estimation for automated 3D kinematic analysis of total knee arthroplasty using X-ray fluoroscopic images, The 25th Annual Congress of the International Society for Technology in Arthroplasty, 2012, Sydney

・医用画像に基づく骨関節３次元動態計測技術と臨床展開，電子情報通信学会医用画像研究会，2012年，山口

H．知的財産権の出願・登録状況　なし

研究報告書

研究成果の刊行に関する一覧表

書籍

著者氏名	論文タイトル名	書籍全体の編集者名	書　籍　名	出版社名	出版地	出版年	ページ

雑誌

発表者氏名	論文タイトル名	発表誌名	巻号	ページ	出版年
T. Yamazaki, et.al	3D Spine Kinematics on Riding Fitness Machines Using 2D/3D Image Registration	IFMBE Proceedings	39	222-225	2012
Nagamoto Y,Ishii T, Iwasaki M, Sakaura H, Moritomo H, Fujimori T, Kashii M, Murase T, Yoshikawa H, Sugamoto K	Three-dimensional motion of the uncovertebral joint during head rotation.	J Neurosurg Spine	7(4)	327-33	2012
Fujimori T, Iwasaki M, Nagamoto Y, Ishii T, Kashii M, Murase T, Sugiura T, Matsuo Y, Sugamoto K, Yoshikawa H.	Kinematics of the thoracic spine in trunk rotation: in vivo 3-dimensional analysis.	Spine (Phila Pa 1976)	37(21)	E1318-28	2012
Fujimori T, Iwasaki M, Nagamoto Y, Kashii M, Ishii T, Sakaura H, Sugamoto K, Yoshikawa H	Three-dimensional measurement of intervertebral range of motion in ossification of the posterior longitudinal ligament: are there mobile segments in the continuous type?	J Neurosurg Spine.	17(1)	74-81	2012

3D Spine Kinematics on Riding Fitness Machines Using 2D/3D Image Registration

T. Yamazaki[1,2], Y. Nagamoto[3], H. Sakaura[4], D. Maeda[5], H. Yoshikawa[4] and K. Sugamoto[3]

[1] The Center for Advanced Medical Engineering and Informatics, Osaka University, Osaka, Japan
[2] Division of Image Analysis, Osaka University Graduate School of Medicine, Osaka, Japan
[3] Division of Orthopaedic Biomaterial Science, Osaka University Graduate School of Medicine, Osaka, Japan
[4] Department of Orthopaedics, Osaka University Graduate School of Medicine, Osaka, Japan
[5] Department of Radiology, Osaka University Hospital, Osaka, Japan

Abstract— **To achieve 3D kinematic analysis of total joint arthroplasty, 2D/3D image registration techniques have attracted attention in recent years. This study presents a 3D spine kinematic measurement method on riding fitness machines using a 2D/3D image registration. First, in order to create the 3D bone model of each spine, CT scan data from a healthy volunteer are used. Next, under fluoroscopic surveillance in the frontal and lateral planes, dynamic spine motions on riding fitness machines are recorded as serial digital x-ray images. 3D poses of each spine are estimated using a feature-based 2D/3D image registration which uses two directional fluoroscopic images and 3D surface model of spine, and finally the 3D kinematics are determined and visualized. In order to validate the accuracy of pose estimation for each spine using a feature-based 2D/3D image registration, computer simulation test was performed. The result showed that the root mean square errors were within 1.0 mm, 1.0 degree for all translations and rotations. In the clinical application 3D spine kinematic analysis using two type of riding fitness machines was successfully performed, and as the results the dynamic movement showed a smooth and reasonable physiologic pattern of motion.**

Keywords— **3D spine kinematics, 2D/3D image registration, Accuracy, X-ray fluoroscopy, Riding fitness machine.**

I. Introduction

To materialize 3D kinematic analysis of various joint including artificial joint implants, previous works have reported some different techniques for measuring the 3D joint kinematics. Video-based motion analysis techniques of skin-mounted markers has been used widely to study gross body motion but less to study detailed joint motion due to the problem of artefacts of skin and soft tissue movement. While, existing accurate 3D measurement techniques, such as computed tomography (CT) and magnetic resonance imaging (MRI), allow assessing movements of the underlying joint directly. However, CT and MRI are not yet capable of achieving high frame rates required for estimating dynamic joint motion, and also the restrictions imposed by the imaging environment (typically a small-diameter cylindrical space) prevent full-motion kinematics measurements.

To eliminate these problems, for kinematic measurement of artificial joint implants, researchers have recently used 3D pose estimation techniques called 2D/3D image registration [1-4], which determine the spatial position and orientation for metallic implants components (e.g. knee, hip, and elbow implants components [5-7]) from X-ray fluoroscopic images and computer aided design (CAD) models of the implants. For normal bones kinematics without artificial joint implants, although a CAD model of the bones is not readily available from the manufacturer, the model can be obtained CT or MRI scan data. Therefore, 3D pose estimation of the normal bones can be achieved. This study presents a 3D spine kinematic measurement method on riding fitness machines using a 2D/3D image registration. We also validate the accuracy of pose estimation for each spine by computer simulation test, and apply the method to dynamic 3D spine kinematic analysis on riding fitness machines.

II. Materials and Metods

A. Condition and requirement

To achieve 3D pose estimation of normal spine using X-ray fluoroscopic images, it is necessary to have an accurate geometrical model of each spine (thoracic, lumbar, and sacral) and to know the geometrical parameters of the X-ray imaging system.

The 3D geometry of each spine is taken from CT scan data. Multidetector computed tomography (MDCT) data, the 0.63 mm axial slice with 512 x 512 image matrix, from a healthy volunteer was used to create 3D bone surface models of thoracic, lumbar, and sacral spine. Segmentation of the bone was performed by applying a thresholding filter. Fig. 1 shows a 3D surface model of normal spine.

The geometrical parameters of the imaging system are determined with a 3D calibration cube and a non-linear calibration technique [8]. The calibration cube has evenly spaced 129 metallic markers, which are employed as calibration markers.

M. Long (Ed.): World Congress on Medical Physics and Biomedical Engineering, IFMBE Proceedings 39, pp. 222–225, 2012.
www.springerlink.com

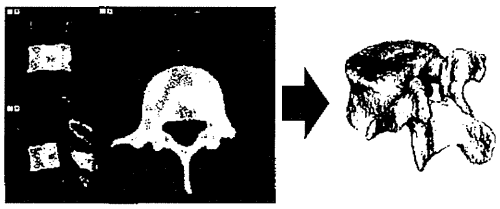

Fig. 1 A spine segmentation and its 3D surface model.

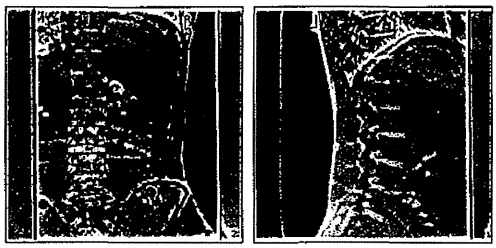

Fig. 2 Frontal and lateral dynamic FPD images of the spine.

B. Image acquisition and processing

Under fluoroscopic surveillance in the frontal and lateral planes, dynamic spine motions on a riding fitness machine were separately recorded as serial digital X-ray images (1024 x 1024 x 12 bits/pixels, 7.5Hz serial spot images as a DICOM file) using a 17-inch dynamic flat-panel detector (FPD) system (C-vision, Shimadzu). This means that two directional X-ray images (approximate bi-plane images) are used to accurately estimate 3D poses of each spine model. To extract the contours of each spine from the acquired image, a Canny's edge detector was applied [9]. Generally, the edges of a fluoroscopic bone image are not sharp like with a metallic implant because of the low contrast of the material. However, use of dynamic FPD images enabled us to easily detect bone edges. False edges and noises detected were manually erased, and the obtained contours were utilized to estimate the 3D pose of the spine model. Fig. 2 shows the frontal and lateral dynamic FPD images of the spine.

C. 2D/3D image registration

3D poses of each spine are estimated using a feature-based 2D/3D image registration [2,4], which uses two directional FPD image contours and 3D bone surface model of each spine. The basic principle of this algorithm is that the 3D pose of a model can be determined by projecting rays from contour points in an image back to the X-ray focus and noting that all of these rays are tangential to the model surface (Fig. 3). Therefore, 3D poses are estimated by minimizing the sum of Euclidean distances between all projected rays and the model surface. A cost function E is defined as the sum of Euclidean distance d_i from point $\mathbf{q}_i$ on the projection rays (corresponding to the point p_i on the contours) to the closest point $\mathbf{s}_i$ on the model surface.

$$E = \sum_{i=1}^{N} d_i^2 \tag{1}$$

The distance d_i is given by

$$d_i = \pm|\mathbf{q}_i - \mathbf{s}_i| \tag{2}$$

where $0 \le i < N$ and N is the number of contour points in the frontal or lateral X-ray images. Negative values indicate rays that cross the model surface. Thus, from single-plane X-ray images, the 3D poses of each spine model are estimated by minimizing the cost function E (equation (1)) iteratively using a nonlinear optimization technique [10]. A good function for determining convergence of the 3D pose of the model from single-plane X-ray images is given by root mean square distance (RMSD):

$$\mathrm{RMSD} = \sqrt{\sum_{i=0}^{N} d_i^2 \Big/ N} \tag{3}$$

Finally, the 3D poses of each spine model are estimated by minimizing the sum of two cost functions using approximate bi-plane images (frontal and lateral images).

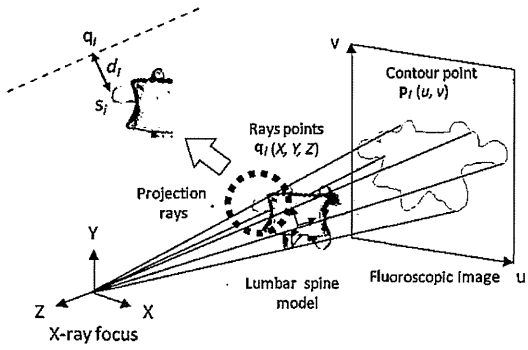

Fig. 3 3D pose estimation of each spine model from a dynamic FPD image.

III. Experimental Results

A. Computer simulation test

In order to validate the accuracy of pose estimation for each spine using a feature-based 2D/3D image registration, computer simulation test was performed. A set of 3 synthetic silhouette images from the frontal and lateral directions was created for each lumbar spine model (L1~L5) in known typical orientations. Ten initial guess poses of each spine model were randomly given from within ±5 mm and ±5 degree of the correct value. Errors in the 3D pose of the model were determined by comparing the estimated pose to the known pose. Fig. 4 shows representative lumbar spine images from the frontal and lateral directions used for computer simulation test.

The results of the computer simulation test are summarized in Table 1. The root-mean-square errors are given for each lumbar spine model (L1~L5). For each spine model, the error of all translations and rotations were within 1.0 mm and 1.0 degree, respectively. For translations, the error of the translation Y was smaller, and for rotations, the error of the rotation X and Z were comparatively smaller. In addition, there were no so differences between the errors of each spine model (L1~L5).

(a) (b)

Fig. 4 Representative lumber spine images used for computer simulation test. (a) frontal view, (b) lateral view.

Table 1 Root-mean-square errors of 3D pose estimation for each lumbar spine model (L1-L5) by computer simulation test.

	Translation (mm)			Rotation (degrees)		
	X	*Y*	*Z*	*X*	*Y*	*Z*
L1	0.50	0.16	0.50	0.29	0.68	0.37
L2	0.73	0.20	0.59	0.23	0.61	0.54
L3	0.98	0.11	0.50	0.20	0.65	0.48
L4	0.73	0.17	0.53	0.17	0.50	0.34
L5	0.91	0.19	0.52	0.21	0.49	0.32

B. Clinical application

We applied the present method to dynamic 3D spine kinematic analysis on riding fitness machines. Experiments were performed using two type of riding fitness machines, products **A** (JOBA EU7800, Panasonic Electric Works) and **B** (RODEOBOY2, Thrive). Both of products **A** and **B** are designed to reproduce motions of a figure of eight, respectively. A healthy male subject gave informed consent to participate in this study, and the study was approved by the authors' Institutional Review Board. 3D kinematics from twelfth thoracic to first sacral spine (total seven vertebras) were determined and visualized.

As the results of the 3D spine kinematics, Fig. 5 visualizes tip motions of the spinous process of thoracic, lumbar, and sacral vertebras from axial view for products **A** and **B**, respectively. The spine kinematics of product **A** clearly showed motions of a figure of eight according to the design concept, but that of product **B** was not observed as motions of a figure of eight. In addition, the spine kinematics of product **A** exhibited large lateral bending and axial rotation compared with that of product **B** as shown in Fig. 6 and 7.

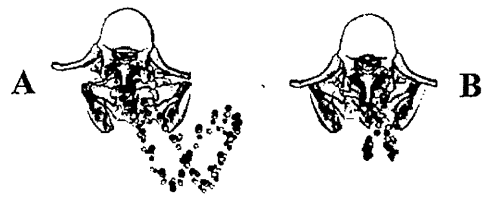

Fig. 5 Tip motions of the spinous process of the vertebras from axial view for products **A** and **B**.

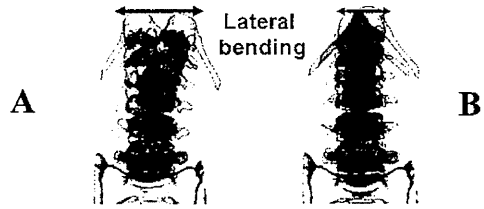

Fig. 6 Lateral bending of the spine for products **A** and **B**.

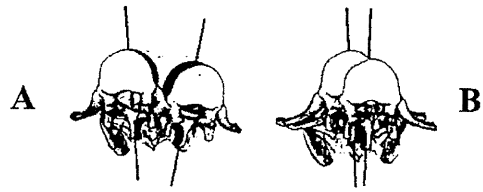

Fig. 7 Axial rotaiton of the spine for products **A** and **B**.

IV. Discussion and conclusions

This study presented a 3D spine kinematic measurement method on riding fitness machines using a feature-based 2D/3D image registration. Utilizing two directional dynamic FPD images (approximate bi-plane images), 3D determination of the spine kinematics was successfully performed.

In computer simulation test, the accuracy of pose estimation for each lumbar spine (L1~L5) were validated, and the error of all translations and rotations were within 1.0 mm and 1.0 degree. Thus, the accuracy of present method was found to be sufficient for analyzing 3D spine kinematics.

In the result of clinical application using two type of riding fitness machines (products **A** and **B**), the spine kinematics of product **A** clearly showed motions of a figure of eight according to the design concept, and then exhibited large lateral bending and axial rotations during spine motions. These large motions might be caused by motions of a figure of eight. Consequently, this type of evaluation is thought to be helpful for developing health and welfare device and assessing its safety and efficiency. As a future work, we are planning to quantitative assessment of 3D spine kinematics including normal joint, joint diseases and dysfunction.

References

1. Banks SA, Hodge WA (1996) Accurate measurement of three-dimensional knee replacement kinematics using single-plane fluoroscopy. IEEE Trans Biomed Eng 43:638-649
2. Zuffi S, Leardini A, Catani F, et al. (1999) A model-based method for the reconstruction of total knee replacement kinematics. IEEE Trans Med Imag 18:981-991
3. Mahfouz MR, Hoff WA, Komistek RD, et al. (2003) A robust method for registration of three-dimensional knee implant models to two-dimensional fluoroscopy images. IEEE Trans Meg Imag 22:1561-1574
4. Yamazaki T, Watanabe T, Nakajima Y, et al. (2004) Improvement of depth position in 2-D/3-D registration of knee implants using single-plane fluoroscopy. IEEE Trans Med Imag 23:602-612
5. Tamaki M, Tomita T, Watanabe T, et al. (2009) In vivo kinematic analysis of a high-flexion, posterior-stabilized, mobile-bearing knee prosthesis in deep knee-bending motion. The Journal of Arthroplasty 24:972-978
6. Koyanagi J, Sakai T, Yamazaki T, et al. (2011) In vivo kinematic analysis of squatting after total hip arthroplasty. Clin Biomech 26:477-483
7. Futai K, Tomita T, Yamazaki T, et al. (2010) In vivo three-dimensional kinematics of total elbow arthroplasty using fluoroscopic imaging. International Orthopaedics 34:847-854
8. Weng J, Cohen P, and Herniou M (1992) Camera calibration with distortion models and accuracy evaluation. IEEE Trans Pattern Anal Machine Intell 14: 965-980
9. Canny J (1986) A computational approach to edge detection. IEEE Trans Pattern Anal Machine Intell 8:679-698
10. Luenberger DG (1984) Linear and Nonlinear Programming. Addison-Wesley, Facsimile edition, Massachusetts

Address of the corresponding author:

Author: Takaharu Yamazaki
Institute: Osaka University
Street: 2-2 Yamadaoka, Suita
City: Osaka
Country: Japan
Email: yamazaki@image.med.osaka-u.ac.jp

J Neurosurg Spine 17:327–333, 2012

Three-dimensional motion of the uncovertebral joint during head rotation

Clinical article

Yukitaka Nagamoto, M.D., Ph.D.,[1] Takahiro Ishii, M.D., Ph.D.,[2] Motoki Iwasaki, M.D., Ph.D.,[1] Hironobu Sakaura, M.D., Ph.D.,[3] Hisao Moritomo, M.D., Ph.D.,[1] Takahito Fujimori, M.D., Ph.D.,[1] Masafumi Kashii, M.D., Ph.D.,[1] Tsuyoshi Murase, M.D., Ph.D.,[1] Hideki Yoshikawa, M.D., Ph.D.,[1] and Kazuomi Sugamoto, M.D., Ph.D.[1]

[1]Department of Orthopaedics, Osaka University Graduate School of Medicine; [2]Department of Orthopaedic Surgery, Kaizuka City Hospital, Osaka; and [3]Department of Orthopaedic Surgery, Kansai Rosai Hospital, Hyogo, Japan

Object. The uncovertebral joints are peculiar but clinically important anatomical structures of the cervical vertebrae. In the aged or degenerative cervical spine, osteophytes arising from an uncovertebral joint can cause cervical radiculopathy, often necessitating decompression surgery. Although these joints are believed to bear some relationship to head rotation, how the uncovertebral joints work during head rotation remains unclear. The purpose of this study is to elucidate 3D motion of the uncovertebral joints during head rotation.

Methods. Study participants were 10 healthy volunteers who underwent 3D MRI of the cervical spine in 11 positions during head rotation: neutral (0°) and 15° increments to maximal head rotation on each side (left and right). Relative motions of the cervical spine were calculated by automatically superimposing a segmented 3D MR image of the vertebra in the neutral position over images of each position using the volume registration method. The 3D intervertebral motions of all 10 volunteers were standardized, and the 3D motion of uncovertebral joints was visualized on animations using data for the standardized motion. Inferred contact areas of uncovertebral joints were also calculated using a proximity mapping technique.

Results. The 3D animation of uncovertebral joints during head rotation showed that the joints alternate between contact and separation. Inferred contact areas of uncovertebral joints were situated directly lateral at the middle cervical spine and dorsolateral at the lower cervical spine. With increasing angle of rotation, inferred contact areas increased in the middle cervical spine, whereas areas in the lower cervical spine slightly decreased.

Conclusions. In this study, the 3D motions of uncovertebral joints during head rotation were depicted precisely for the first time.

(http://thejns.org/doi/abs/10.3171/2012.6.SPINE111104)

Key Words • **uncovertebral joint** • **three-dimensional kinematics** • **head rotation** • **volume registration** • **cervical**

The uncovertebral joints (Luschka joints) are small but clinically important anatomical structures of the cervical vertebrae. Each joint consists of the uncinate process and corresponding recess located on the inferolateral surface of the superior adjacent vertebral body. In the aged or degenerative cervical spine, osteophytes arising from an uncovertebral joint can cause cervical radiculopathy, often requiring decompression surgery. Although the biomechanical roles[1,13,18,19,24] and morphological characteristics[4,6,14,17] of the uncovertebral joints have been investigated, the functions of uncovertebral joints have yet to be definitively clarified. Full elucidation of the function, including kinematics, of the uncovertebral joints is thus very important.

According to previous comparative anatomical investigations, uncinate processes are found only in ob-

This article contains some figures that are displayed in color online but in black-and-white in the print edition.

ligate or facultative bipedal animals, such as primates, marsupials, and rodents.[7] In the upright position, rotation of the cervical spine is needed to allow the animal to look around. From this anatomical observation, uncovertebral joints are believed to play some role in head rotation.[17,19] To the best of our knowledge, however, no studies have reported kinematics of the uncovertebral joints during head rotation. We have developed a 3D imaging system to noninvasively evaluate relative motions of individual cervical vertebrae in vivo.[8–10] The purpose of this study was to elucidate 3D motion of the uncovertebral joints to provide a better understanding of the function of these joints during head rotation.

Methods

Study Population

Study participants were 10 healthy volunteers (5 men and 5 women) with neither neck pain nor a medical history of cervical spine disorders. Mean age at the time of imaging was 25.1 years (range 22–31 years). All study protocols were approved by the institutional review board. Informed consent was obtained in all volunteers.

Acquisition of 3D MRI

Each volunteer was placed supine on the MRI table and underwent 3D MRI in 11 positions with the head rotated: 0° (neutral), 15°, 30°, 45°, and 60°, and maximum rotation to each side (left and right). We instructed all volunteers to rotate the head as perpendicularly as possible about the axis of the body trunk. The shoulders of each volunteer were fixed to the table using a band. All 3D MRI scans were acquired using a 1.0-T commercial MRI system (Signa LX, General Electric) in conjunction with a torso-phased array coil. A 3D fast-gradient recalled acquisition in the steady state (GRASS) sequence was used (TR 8.0 msec, TE 3.3 msec, slice thickness 1.5 mm, no interslice gap, flip angle 10°, FOV 24 cm, inplane acquisition matrix 256 × 224). Magnetic resonance imaging data were saved in DICOM format and transmitted to a computer workstation, where image processing was performed using software developed in our laboratory (Virtual Place M series, Medical Imaging Laboratory).

Motion Analysis

Our original method used in the present study has been fully described in previous reports[8–10] and will be described here only briefly. First, regions of interest were extracted in 3D from the 3D MRI data (segmentation) and 6 vertebrae from C-2 to C-7 were extracted semiautomatically using an intensity threshold technique. Second, using a volume registration method,[8–10] 3D motions of each vertebra in an absolute coordinate system were calculated by automatically superimposing the segmented region of each vertebra on 3D MRI in the neutral position over images of every position. Intervertebral motions of every motion segment from C2–3 to C6–7 were then calculated by converting the absolute motion (3 × 4 matrix) obtained from the preceding image processing into a relative motion with respect to the subjacent vertebra. These motions were expressed in 6 df by Euler angles with the sequence of pitch (X), yaw (Y), roll (Z), and translations using a previously defined anatomical coordinate system.[8–10] Accuracy of this method was as follows: 0.24° for flexion-extension, 0.31° for lateral bending, 0.43° for axial rotation, 0.52 mm for superoinferior translation, 0.51 mm for anteroposterior translation, and 0.41 mm for lateral translation, as described in detail previously.[10]

Creation of 3D Bone Models

Surface bone models constructed from 3D MRI data provided insufficient information on configuration to investigate in vivo 3D kinematics of the uncovertebral joint, due to a lack of spatial resolution. We therefore decided to choose surface bone models from multidetector row CT (LightSpeed 16, General Electric) for analysis, and these models reproduced anatomical structures much more accurately than models from 3D MRI. Computed tomography data for the cervical spine were selected from the DICOM server at our institution, based on anatomical characteristics described in several studies of the uncovertebral joints.[4,6,14,17,18] The source of the data was a 28-year-old man who was not part of the 10-patient cohort. More specifically, characteristics of the selected CT data were as follows: the uncinate processes situated laterally at middle cervical levels (C2–3, C3–4, C4–5) and dorsolaterally at lower cervical levels (C5–6, C6–7)[6,17] demonstrated reduced height of the processes in relation to the vertebral bodies at lower cervical levels (Fig. 1).[4,14] Regarding sagittal orientation of facets, facet slope is more gradual as the cervical level descends caudally. There were no degenerative changes, and normal disc heights were maintained at all levels on conventional 2D MRI. In this way, 6 surface bone models from C-2 to C-7 were created.

Three-Dimensional Visualization of Motion

All intervertebral motions from the 10 volunteers were aggregated and standardized at every intervertebral level using our original operation algorithm. The results of standardized 3D intervertebral motions were expressed as matrices. A pair of CT vertebral models of a functional spinal unit was displayed in virtual 3D space, allowing us to obtain a 3D movie of intervertebral motions by introducing the matrices to the superior adjacent vertebra alone and keeping the subjacent vertebra fixed (Fig. 2, Video 1).

> Video 1. Clip showing 3D motion of the uncovertebral joints. This 3D animation of the uncovertebral joints during head rotation shows joints alternating between contact and separation accompanying torsion of the intervertebral space. To allow a better understanding of intervertebral motions, the subjacent vertebra is always fixed in this clip. For example, C-3 is fixed in the clip showing C2–3. Click here to view with Media Player. Click here to view with Quicktime.

Creation of the animation was accomplished using originally developed software (Orthopedics Viewer, Osaka University) that allowed the observer to closely examine every uncovertebral joint from every observation point needed. These 3D animations helped us to better understand the joint kinematics.

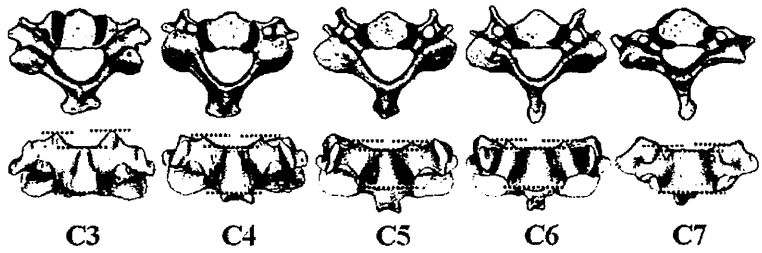

FIG. 1. Surface bone models created using CT data. We chose CT data with the following anatomical characteristics: uncinate processes situated laterally at middle cervical levels (C3–4) and dorsolaterally at lower cervical levels (C5–7), represented in the upper row as *dark gray* areas, as well as relatively reduced height of the processes at lower cervical levels, represented in the lower row as *dashed lines*.

Contact Area

We measured inferred contact areas of the uncovertebral joints during head rotation from bone surface models using a proximity mapping method.[16] Proximity mapping involves the visualization of distance from 1 bone to the nearest neighboring bone. We defined the area within a preset interbone distance as the inferred contact area. Contact areas were investigated at 15° increments during head rotation at every intervertebral level from C2–3 to C6–7 (Fig. 3, Video 2).

VIDEO 2. Clip showing inferred contact area of the uncovertebral joint. The inferred contact areas of the uncinate processes during head rotation were situated directly lateral at the middle cervical spine and dorsolateral at the lower cervical spine. Click here to view with Media Player. Click here to view with Quicktime.

Thresholds of preset interbone distances varied within 0.5–1.0 mm according to the individual joint size and intervertebral space.

Results

Intervertebral Motion

In main axial rotation, C4–5 and C5–6 were the most mobile segments and C2–3 was the least mobile segment, as previously reported (Table 1). During head rotation, larger rotation angles were observed in coupled lateral bending than in main axial rotation in all segments, and C2–3 and C3–4 were the most mobile segments in coupled lateral bending, despite the immobility in axial rotation (Table 2).

Behavior of Uncovertebral Joints

The 3D animation of uncovertebral joints during head rotation showed joints alternating between contact and separation accompanying torsion of the intervertebral space. On the side ipsilateral to head rotation, both joint surfaces were in contact with each other, while those on the contralateral side were separated (Fig. 2, Video

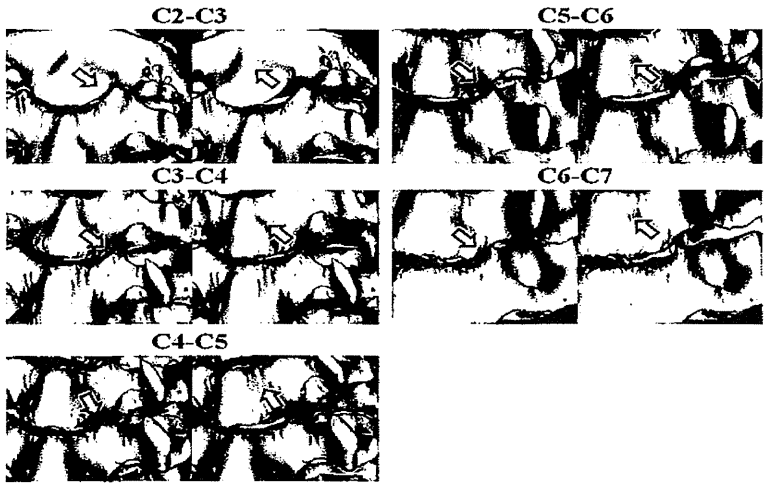

FIG. 2. The behaviors of uncovertebral joints were shown in a 3D animation. Each paired image focuses on the left uncovertebral joint from a left anterior oblique view. *Downward arrows* show contact and *upward arrows* show separation of the joint. For each level, left panels represent head rotation to the left, and right panels represent head rotation to the right.

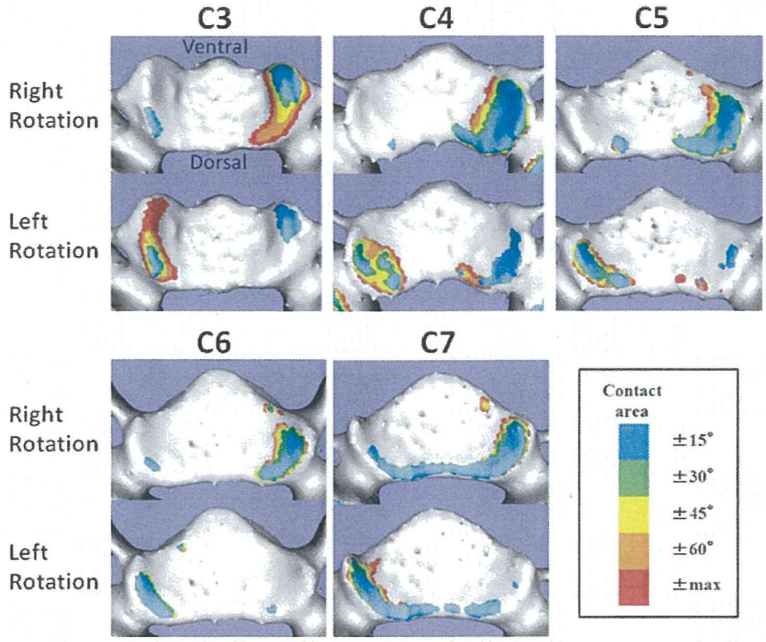

FIG. 3. Inferred contact areas projected on the uncinate process side. Each panel represents a cranial view with the upper part of each panel as the ventral side. Inferred contact areas are shown using 5 different colors, as shown in the **key**.

1). This pattern of motion was strongly apparent in the middle cervical spine, especially at the C2–3 level.

Contact Areas for Uncovertebral Joints

Inferred contact areas of the uncovertebral joints are shown in Fig. 3 and Video 2. Inferred contact areas showed that the uncovertebral joints were the first contact areas in the intervertebral space during head rotation and were situated directly lateral at the middle cervical spine and dorsolateral at the lower cervical spine. The dimensions (mm^2) of inferred contact areas were also calculated (Fig. 4). With increasing rotation angle of the head, inferred contact areas increased in the middle cervical spine, but slightly decreased in the lower cervical spine.

Discussion

Roles for Uncovertebral Joints and Uncinate Processes During Head Rotation

During head rotation, lateral flexion is coupled with rotation in the cervical spine and is called "coupled motion." Facet joints undoubtedly represent the biggest contributors to such motion, due to their oblique orientation.[9,18] In addition, several studies have suggested the contribution

TABLE 1: Intervertebral motion during head rotation: main axial rotation*

Head Rotation Angle (°)	C2–3	C3–4	C4–5	C5–6	C6–7
rt max	−2.3 ± 1.2	−4.7 ± 1.0	−4.9 ± 1.3	−4.5 ± 0.8	−2.6 ± 0.7
rt 60	−1.5 ± 0.9	−3.6 ± 0.8	−4.0 ± 1.2	−3.8 ± 0.6	−2.3 ± 0.5
rt 45	−0.7 ± 0.8	−2.3 ± 0.5	−2.7 ± 1.3	−2.9 ± 0.4	−2.0 ± 0.8
rt 30	−0.2 ± 0.7	−1.0 ± 0.7	−1.7 ± 1.1	−1.9 ± 0.7	−1.2 ± 0.9
rt 15	0.0 ± 0.7	−0.2 ± 0.5	−0.8 ± 0.5	−1.3 ± 0.7	−1.0 ± 0.9
lt 15	−0.4 ± 0.6	0.2 ± 0.7	0.9 ± 0.5	1.6 ± 1.2	0.7 ± 1.1
lt 30	0.2 ± 0.4	1.1 ± 0.9	1.4 ± 0.5	1.8 ± 1.4	1.0 ± 1.4
lt 45	0.4 ± 0.5	2.0 ± 0.9	2.1 ± 0.7	2.4 ± 1.4	1.2 ± 0.9
lt 60	1.1 ± 0.7	2.9 ± 1.0	3.1 ± 0.9	3.3 ± 1.5	2.1 ± 1.0
lt max	1.5 ± 0.6	3.8 ± 1.0	3.9 ± 1.1	4.0 ± 1.5	2.4 ± 0.9

* All values given in mean degrees ± SD. Negative values = right axial rotation; positive values = left axial rotation.

TABLE 2: Intervertebral motion during head rotation: coupled lateral bending*

Head Rotation Angle (°)	C2–3	C3–4	C4–5	C5–6	C6–7
rt max	4.0 ± 1.3	6.2 ± 1.1	5.7 ± 1.1	5.6 ± 1.2	4.9 ± 1.8
rt 60	2.5 ± 1.3	5.0 ± 1.2	4.4 ± 1.3	4.9 ± 1.1	3.6 ± 1.4
rt 45	0.6 ± 1.0	3.1 ± 1.2	3.5 ± 1.2	3.0 ± 1.2	2.5 ± 1.7
rt 30	−0.6 ± 1.7	1.8 ± 1.2	1.9 ± 1.0	2.4 ± 1.3	1.7 ± 1.9
rt 15	−0.9 ± 1.6	0.7 ± 0.9	1.3 ± 0.8	1.2 ± 1.5	1.3 ± 1.2
lt 15	1.4 ± 2.1	−0.4 ± 0.9	−1.7 ± 1.3	−1.2 ± 1.3	−1.6 ± 2.7
lt 30	0.4 ± 2.0	−1.4 ± 0.8	−1.6 ± 1.1	−2.2 ± 1.9	−1.2 ± 1.9
lt 45	−0.8 ± 2.2	−2.3 ± 0.8	−2.6 ± 0.8	−2.6 ± 1.7	−2.5 ± 2.0
lt 60	−2.0 ± 2.1	−3.7 ± 1.2	−3.7 ± 0.7	−3.7 ± 1.3	−3.1 ± 2.3
lt max	−3.5 ± 1.8	−5.0 ± 1.2	−4.8 ± 1.0	−4.6 ± 1.4	−4.3 ± 2.2

* All values given in mean degrees ± SD. Negative values = left lateral bending; positive values = right lateral bending.

of uncinate processes to coupled motion.[1,7,18,19] Hall[7] noted that among vertebrates, uncinate processes on the cervical vertebrae are found only in obligate or facultative bipeds, which require rotation of the neck to look around. Given these findings, he hypothesized that the uncovertebral joints arose during evolution from quadrupedalism to bipedalism, and bear some relationship to neck rotation. To verify Hall's hypothesis, Penning and Wilmink[19] calculated the axis of rotation from the anatomical shape of uncovertebral joints, using CT sections in the plane of the facet joints in 2 different positions. These authors showed that coupling of lateral bending and rotation of the middle and lower cervical spine might be explained exclusively by the axis and morphological structure of the uncovertebral joints, and that the uncinate processes are also essential for rotation. Clausen et al.[1] quantitatively investigated contributions of the uncovertebral joints to motion of a spinal segment, including axial rotation, for the first time. Using finite element models, they elucidated that the presence of the uncovertebral joint (a fissure) leads to increased motions, while the uncinate processes act as stabilizers with respect to motion of the cervical spinal segment, particularly during axial rotation and lateral bending of the cervical spine.[1] However, that study was performed using only computer simulations, and the acquired data were not derived from real sources. Moreover, they analyzed kinematics only at the C5–6 segment, whereas anatomical variations at different vertebral levels may influence cervical biomechanics.

In our study, with increasing angle of head rotation, two opposite surfaces of the uncovertebral joint became closer and closer on the ipsilateral side of rotation, while surfaces on the contralateral side became more and more separated. This pattern was strongly observed in the middle cervical spine. Moreover, at these levels, inferred contact areas were situated directly lateral and increased with increasing angle of rotation, particularly at C2–3. In the middle cervical spine, larger coupled lateral bending would accompany head rotation, as these levels show a steeper sagittal inclination of facets than those of the lower cervical spine.[11] Taking these findings together, we speculated that the presence of large processes relative to the vertebral body[14] might restrict excessive coupled lateral bending and disperse mechanical stresses effectively on large joint surfaces in the middle cervical spine. In fact, the C2–3 segment, which has the largest uncinate process, had the smallest motion in terms of both main axial rotation and coupled lateral bending in our study.

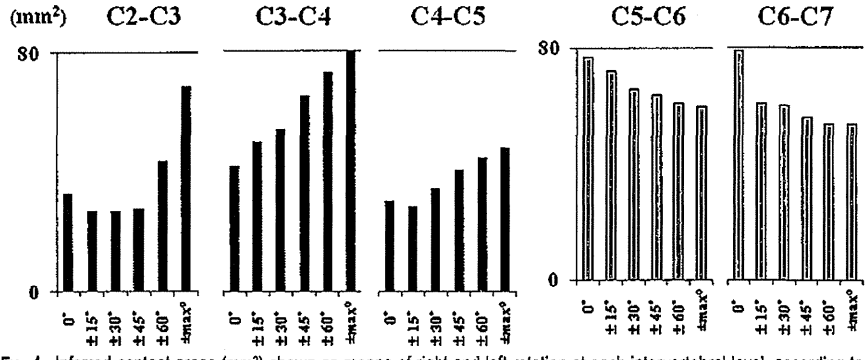

FIG. 4. Inferred contact areas (mm²) shown as means of right and left rotation at each intervertebral level, according to the angle of head rotation. With increasing rotation angle of the head, inferred contact areas increased in the middle cervical spine, but slightly decreased in the lower cervical spine.

Conversely, in the lower cervical spine, the inferred contact areas were situated dorsolaterally and these areas slightly decreased with increasing angle of rotation. Focusing only on the shape of the uncinate processes in the lower cervical spine, which displays more gradual inclination of facets than those of the middle cervical spine, axial rotation should be allowed without large coupled lateral bending. Therefore, the uncinate processes of the lower cervical spine might play a less important role in restricting excessive coupled lateral bending than those of the middle cervical spine. Given this observation, we speculated that uncinate processes of the lower cervical spine might not have to be as large as those of the middle cervical spine and instead play an important role in facilitating rotation of the cervical spine by placing the stress-focusing region on the posterolateral side of the upper surfaces of the vertebrae.

Nerve Root Compression and Uncovertebral Osteophytes in the Lower Cervical Spine

Cervical radiculopathy is often related to osteophyte formation around the uncinate process; C-7 root lesions are the most common, followed by C-6 lesions.[20,21] A longer course of the nerve root in close proximity to the uncovertebral joint may explain the predisposition toward nerve root compression by uncovertebral osteophytes at these levels.[3] However, anatomical or biomechanical reasons for a predisposition toward uncovertebral osteophytes in the lower cervical spine remain unclear.

In the present study, we elucidated that the uncovertebral joints are the first contact areas in the intervertebral space during head rotation. From these results, we speculated that as disc height diminishes with degeneration, earlier contact should occur around the uncovertebral joints during head rotation, and would be likely to promote age-related degenerative change around the uncovertebral joints due to the increased frequency of mechanical stress. If the degenerated disc causes abnormal intervertebral kinematics, further degenerative changes around the uncovertebral joints would occur. The lower cervical spine is well-known as the level most commonly affected by aging,[2,5,15,22] and moreover, inferred contact areas of the uncovertebral joints at the lower cervical spine were situated dorsolaterally and decreased with increasing angle of rotation. These contact areas are closer to the course of the nerve root than in the middle cervical spine and may be subjected to strong mechanical stress, because stresses are focused in such small areas. The accumulation of mechanical stress in joints induces osteophyte formation.[12] Head axial rotation movements are often repeated during activities of daily living.[23] Repeated head rotation in the course of activities of daily living might thus contribute to spur formation around contact areas of the uncovertebral joints in the lower cervical spine close to the intervertebral foramen. This speculative situation would account for the fact that cervical radiculopathy generally occurs in the lower cervical spine, particularly C5–6 and C6–7.

Limitations of the Study

Several limitations in this study must be addressed. First, information was obtained from animations (Videos 1 and 2) comprising only 11 different positions and could not be obtained with the volunteer in an upright position. Second, individual variability in uncovertebral joints6 could not be taken into account, even though these variations are likely to affect kinematics. Moreover, the surface bone models were constructed using data from a volunteer outside the 10-patient cohort. We acknowledge that this method includes the potential for bias. Third, contact areas of the uncovertebral joints were not "true" (verified), but were instead inferred. The presence of intervening tissues such as discs, joint cartilages, and synovial fluids were not taken into account. And fourth, contact pressure and pressure distributions could not be measured using our methods. Despite all these limitations, we believe that no other approaches currently allow the investigation of 3D motion of the uncovertebral joints in healthy individuals. The present study thus offers a step toward a better understanding of functions of the uncovertebral joints.

Conclusions

We have shown 3D motion of the uncovertebral joints during head rotation for the first time. Standardized 3D intervertebral motions of the cervical spine showed that the uncovertebral joints alternate between contact and separation during head rotation. Inferred contact areas of uncovertebral joints were situated directly lateral at the middle cervical spine and dorsolateral at the lower spine. With increasing angles of rotation, inferred contact areas increase in the middle cervical spine, particularly at C2–3, whereas areas slightly decrease in the lower cervical spine.

Disclosure

The authors report no conflict of interest concerning the materials or methods used in this study or the findings specified in this paper.

Author contributions to the study and manuscript preparation include the following. Conception and design: Nagamoto, Iwasaki, Moritomo. Acquisition of data: Nagamoto, Ishii. Analysis and interpretation of data: Nagamoto, Sakaura. Drafting the article: Nagamoto. Critically revising the article: all authors. Reviewed submitted version of manuscript: all authors. Approved the final version of the manuscript on behalf of all authors: Nagamoto. Administrative/technical/material support: Iwasaki, Murase, Yoshikawa, Sugamoto. Study supervision: Iwasaki, Murase, Yoshikawa, Sugamoto.

Acknowledgments

The authors thank Ryoji Nakao for assisting with software programming and Yoshihiro Sakaguchi for help with MRI.

References

1. Clausen JD, Goel VK, Traynelis VC, Scifert J: Uncinate processes and Luschka joints influence the biomechanics of the cervical spine: quantification using a finite element model of the C5-C6 segment. **J Orthop Res 15:**342–347, 1997
2. Dvorak J, Panjabi MM, Grob D, Novotny JE, Antinnes JA: Clinical validation of functional flexion/extension radiographs of the cervical spine. **Spine (Phila Pa 1976) 18:**120–127, 1993
3. Ebraheim NA, Lu J, Biyani A, Brown JA, Yeasting RA:

Anatomic considerations for uncovertebral involvement in cervical spondylosis. **Clin Orthop Relat Res (334):**200–206, 1997
4. Ebraheim NA, Xu R, Bhatti RA, Yeasting RA: The projection of the cervical disc and uncinate process on the posterior aspect of the cervical spine. **Surg Neurol 51:**363–367, 1999
5. Friedenberg ZB, Edeiken J, Spencer HN, Tolentino SC: Degenerative changes in the cervical spine. **J Bone Joint Surg Am 41-A:**61–70, 1959
6. Frykholm R: Lower cervical vertebrae and intervertebral discs; surgical anatomy and pathology. **Acta Chir Scand 101:**345–359, 1951
7. Hall M: **Luschka's Joint.** Springfield, IL: C.C. Thomas, 1965
8. Ishii T, Mukai Y, Hosono N, Sakaura H, Fujii R, Nakajima Y, et al: Kinematics of the cervical spine in lateral bending: in vivo three-dimensional analysis. **Spine (Phila Pa 1976) 31:**155–160, 2006
9. Ishii T, Mukai Y, Hosono N, Sakaura H, Fujii R, Nakajima Y, et al: Kinematics of the subaxial cervical spine in rotation in vivo three-dimensional analysis. **Spine (Phila Pa 1976) 29:**2826–2831, 2004
10. Ishii T, Mukai Y, Hosono N, Sakaura H, Nakajima Y, Sato Y, et al: Kinematics of the upper cervical spine in rotation: in vivo three-dimensional analysis. **Spine (Phila Pa 1976) 29:**E139–E144, 2004
11. Kapanji AI: **The Physiology of the Joints, Volume Three: The Spinal Column, Pelvic Girdle and Head, ed 6.** New York: Churchill Livingstone, 2008
12. Kawaguchi H: Endochondral ossification signals in cartilage degradation during osteoarthritis progression in experimental mouse models. **Mol Cell 25:**1–6, 2008
13. Kotani Y, McNulty PS, Abumi K, Cunningham BW, Kaneda K, McAfee PC: The role of anteromedial foraminotomy and the uncovertebral joints in the stability of the cervical spine. A biomechanical study. **Spine (Phila Pa 1976) 23:**1559–1565, 1998
14. Milne N: The role of zygapophysial joint orientation and uncinate processes in controlling motion in the cervical spine. **J Anat 178:**189–201, 1991
15. Miyazaki M, Hong SW, Yoon SH, Zou J, Tow B, Alanay A, et al: Kinematic analysis of the relationship between the grade of disc degeneration and motion unit of the cervical spine. **Spine (Phila Pa 1976) 33:**187–193, 2008
16. Moritomo H, Viegas SF, Elder KW, Nakamura K, Dasilva MF, Boyd NL, et al: Scaphoid nonunions: a 3-dimensional analysis of patterns of deformity. **J Hand Surg Am 25:**520–528, 2000
17. Panjabi MM, Duranceau J, Goel V, Oxland T, Takata K: Cervical human vertebrae. Quantitative three-dimensional anatomy of the middle and lower regions. **Spine (Phila Pa 1976) 16:**861–869, 1991
18. Penning L: Differences in anatomy, motion, development and aging of the upper and lower cervical disk segments. **Clin Biomech (Bristol, Avon) 3:**37–47, 1988
19. Penning L, Wilmink JT: Rotation of the cervical spine. A CT study in normal subjects. **Spine (Phila Pa 1976) 12:**732–738, 1987
20. Polston DW: Cervical radiculopathy. **Neurol Clin 25:**373–385, 2007
21. Radhakrishnan K, Litchy WJ, O'Fallon WM, Kurland LT: Epidemiology of cervical radiculopathy. A population-based study from Rochester, Minnesota, 1976 through 1990. **Brain 117:**325–335, 1994
22. Shedid D, Benzel EC: Cervical spondylosis anatomy: pathophysiology and biomechanics. **Neurosurgery 60 (1 Suppl 1):** S7–S13, 2007
23. Sterling AC, Cobian DG, Anderson PA, Heiderscheit BC: Annual frequency and magnitude of neck motion in healthy individuals. **Spine (Phila Pa 1976) 33:**1882–1888, 2008
24. White AA III, Panjabi M: **Clinical Biomechanics of the Spine, ed 2.** Philadelphia: Lippincott Williams & Wilkins, 1990

Manuscript submitted January 27, 2012.
Accepted June 28, 2012.
Portions of this study were presented on December 3, 2009, during the podium session at the 37th Annual Meeting of the Cervical Spine Research Society, Salt Lake City, Utah.
Please include this information when citing this paper: published online August 3, 2012; DOI: 10.3171/2012.6.SPINE111104.
Supplemental online information:
Video 1: http://mfile.akamai.com/21490/wmv/digitalwbc.download.akamai.com/21492/wm.digitalsource-na-regional/spine11-1104_video_1.asx (Media Player).
http://mfile.akamai.com/21488/mov/digitalwbc.download.akamai.com/21492/qt.digitalsource-global/spine11-1104_video_1.mov (Quicktime).
Video 2: http://mfile.akamai.com/21490/wmv/digitalwbc.download.akamai.com/21492/wm.digitalsource-na-regional/spine11-1104_video_2.asx (Media Player).
http://mfile.akamai.com/21488/mov/digitalwbc.download.akamai.com/21492/qt.digitalsource-global/spine11-1104_video_2.mov (Quicktime).
Address correspondence to: Yukitaka Nagamoto, M.D., Ph.D., Department of Orthopaedics, Osaka University Graduate School of Medicine, 2-2 Yamadaoka, Suita, Osaka 565-0871, Japan. email: 7gam0to@gmail.com.

Spine

SPINE Volume 37, Number 21, pp E1318–E1325

BIOMECHANICS

Kinematics of the Thoracic Spine in Trunk Rotation

In Vivo 3-Dimensional Analysis

Takahito Fujimori, MD, PhD,* Motoki Iwasaki, MD, PhD,* Yukitaka Nagamoto, MD, PhD,* Takahiro Ishii, MD, PhD,† Masafumi Kashii, MD, PhD,* Tsuyoshi Murase, MD, PhD,* Tsuyoshi Sugiura, MD,* Yohei Matsuo, MD,* Kazuomi Sugamoto, MD, PhD,‡ and Hideki Yoshikawa, MD, PhD*

Study Design. *In vivo* 3-dimensional (3D) study of the thoracic spine.

Objective. To demonstrate axial rotations (ARs) and coupled motions of the thoracic spine.

Summary of Background Data. *In vivo* 3D kinematics of the thoracic spine in trunk rotation with intact thorax and soft tissues has not been well-known.

There were no quantitative data of AR in the consecutive thoracic spinal segments. Patterns of coupled motion with AR have been controversial.

Methods. Thirteen healthy volunteers underwent 3D computed tomography of the thoracic spine in 3 positions; neutral, right, and left maximum trunk rotation. Relative motions of vertebrae were calculated by automatically superimposing the vertebrae in a neutral position over images in rotational positions, using voxel-based registration. Motions were represented with 6 degrees of freedom by Euler angles and translations on the local coordinate system.

Results. Mean (±SD) relative rotational angles of T1 with respect to L1 to 1 side were 24.9° ± 4.9° in maximum trunk rotation. AR of each thoracic segment with respect to the inferior adjacent vertebra to 1 side was 1.2° ± 0.8° at T1–T2, 1.6° ± 0.7° at T2–T3, 1.4° ± 0.9° at T3–T4, 1.6° ± 0.8° at T4–T5, 1.8° ± 0.7° at T5–T6, 1.9° ± 0.6° at T6–T7, 2.3° ± 0.7° at T7–T8, 2.5° ± 0.8° at T8–T9, 2.7° ± 0.6° at T9–T10, 2.6° ± 0.8° at T10–T11, 1.3° ± 0.7° at T11–T12, and 0.5° ± 0.4° at T12–L1. Significantly larger segmental AR was observed at the middle thoracic segments (T6–T11) than at the upper (T1–T6) and lower (T11–L1) segments. At the upper thoracic segments, coupled lateral bending with AR was observed in the same direction as AR. However, at the middle and lower thoracic segments, coupled lateral bending occurred both in the same and opposite directions.

Conclusion. *In vivo* 3D ARs and coupled motions of the consecutive thoracic spinal segments in trunk rotation were investigated accurately for the first time.

Key words: thoracic spine, rotation, coupling motion, *in vivo*, 3-dimensional. **Spine 2012;37:E1318–E1328**

Spinal biomechanics and kinesiology are essential for better comprehension of the pathogenesis of spinal disorders and therapies. Relationships between biomechanics and spinal disorders have been discussed in previous research.[1] Compared with other regions of the spine, the thoracic spine is unique in both anatomy and potential disorders. The disc of the thoracic spine represents a reduced amount of height in ratio to the vertebral body, and the angle of facet joints is steeper than the cervical spine and is more frontally oriented than the lumbar spine. Many spinal traumas occur in the thoracolumbar region and scoliotic deformity frequently starts in the midthoracic region. Correction of rotational deformity of scoliosis is a technically demanding procedure[2]; however, it is not well-known how much axial rotation (AR) could physiologically occur in the normal thoracic spine. The kinematics of the thoracic spine has been investigated on *in vitro* cadaveric studies[3–5] and mathematical models[6] and *in vivo* by using the 3-space track system[7–8] or invasive pin insertion method.[9–10] Although cadaver studies and mathematical models enabled accurate measurement, they might not be physiological in relation to the lack of rib cage, real muscle tone, or intra-abdominal pressure. In many cadaver studies, analysis was performed in various spinal units of limited numbers on elderly subjects. The decision of whether to simulate ideal force or torque *in vivo* motions may be difficult. The 3-space track system was a noninvasive method; however, it was difficult to assess intervertebral motions of each single spinal segment because of the potential for measurement errors.[11] Measurement by the pin insertion method was accurate and physiological; however, it seemed to be too invasive to be performed at each spinal segment. Thus, *in vivo* 3-dimensional

From the *Departments of Orthopedic Surgery; †Department of Orthopedic Surgery, Kaizuka City Hospital, Osaka, Japan; and ‡Orthopedic Biomaterial Science, Osaka University Graduate School of Medicine, Osaka, Japan.

Acknowledgment date: April 30, 2012. Revision date: June 18, 2012. Acceptance date: June 22, 2012.

The manuscript submitted does not contain information about medical devices or drugs.

This work was supported by a grant-in-aid for Scientific Research C (KAKENHI: 22591632) from the Ministry of Education, Culture, Sports, and Technology, Japan; and by an AO Spine research grant.

No benefits in any form have been or will be received from a commercial party related directly or indirectly to the subject of this manuscript.

Address correspondence and reprint requests to Takahito Fujimori, MD, PhD, Department of Orthopaedic Surgery, Osaka University Graduate School of Medicine, 2–2 Yamadaoka, Suita, Osaka 565–0871, Japan; E-mail: takahito-f@hotmail.co.jp

DOI: 10.1097/BRS.0b013e318267254b

(3D) motions at each consecutive segment of the thoracic spine have been unknown. The purpose of our study was to demonstrate *in vivo* within each intervertebral and coupled motion of the thoracic spine in trunk rotation by using the 3D imaging technique.

MATERIALS AND METHODS

Our study participants were 13 healthy male volunteers. Subjects with a history of spinal disorders, spinal surgery, lung disease, or anything that could affect spinal biomechanics were excluded. Subjects were not athletes or gymnasts. No scoliotic curve greater than 5° was found. All study protocols were approved by our institutional review board, and study participants provided written informed consent after receiving detailed information about the study.

Measurement of Intervertebral Range of Motion

Acquisition of 3D Computed Tomography

Low-dose functional computed tomographic (CT) scans were obtained for 3 positions for each subject using a commercial CT system (LightSpeed, GE Healthcare, Milwaukee, WI) with the following parameters: slice thickness, 0.625 mm; pixel size, 0.352 mm; tube rotation speed, 0.5 seconds; beam collimation, 40 mm; beam pitch, 0.9; tube current, 20 mA; and voltage, 120 kV. Subjects were placed in a neutral position that was defined as being supine on the flat CT table in a relaxed manner. The subjects' arms were held behind their heads and the pelvis was tightly fixed to the table with a belt to keep both sides of anterior-superior iliac spines parallel to the table (Figure 1). Subjects were instructed to actively rotate their shoulder girdles along with the axis of the body trunk. Rotational positions were defined as twisting the trunk at a maximum to the right and left side within a range that subjects did not feel pain or discomfort. A soft cushion device was used for the trunk to support the rotational position and for the head to be kept in the neutral position. To reduce radiation exposure, scans done in rotational positions were performed with a lower tube current, 10 mA. Total exposure was 350 dose-length products, which is less than that specified for a routine whole-spine CT by our hospital. CT data were transferred *via* digital imaging and communications in medicine network into a computer workstation, where image processing was performed using Virtual Place software (M series, Medical Imaging Laboratory, Tokyo, Japan).

Motion Analysis

The method used was fully described in our previous reports. Contour of each vertebra was semiautomatically extracted from CT at a specific threshold. A bone window with a width of 2000 Hounsfield units and a level of 150 Hounsfield units was used for the threshold. The segmented vertebra in the neutral position was automatically superimposed on other positions by voxel-based registration. The migration was represented as a matrix. This matrix was converted into the matrix representing relative motion with respect to the inferior adjacent vertebra on the local coordinate axis. The local coordinate axis of the vertebra was defined as the right-handed orthogonal axis system in accordance with the definition provided by the Scoliosis Research Society working group (Figure 2).[12] Three-dimensional motion of each vertebra relative to the inferior adjacent vertebra was expressed in 6 degrees of freedom by Euler angles with the sequence of roll (*X*), pitch (*Y*), yaw (*Z*) in accordance with the results reported by Skalli *et al.*[13] For better understanding, relative motion of T1 vertebra with respect to L1 vertebra was also computed.

Accuracy

The accuracy of this analysis system was: 0.19° in flexion-extension, 0.13° in AR, 0.21° in lateral bending (LB), 0.13 mm in lateral translation, 0.15 mm in superoinferior translation, and 0.31 mm in anteroposterior translation, as described in detail previously.[14]

Statistical Analysis

Mean and SD for range of motion (ROM) to 1 side were computed. The thoracic spine was divided into 3 parts, upper segments: T1–T2 to T5–T6; middle segments: T6–T7 to T10–T11; and lower segments: T11–T12 to T12–L1. ARs of these segments were compared using the unpaired *t* test. The frequency of coupled LB to the same direction as AR among subjects was compared using Kruskal-Wallis rank sum test. JMP software (version 8.0.1; SAS Institute, Cary, NC) was used for statistical analysis. *P* values of less than 0.05 were considered to indicate statistical significance.

RESULTS

Data of Participants

Mean age, height, body weight, and body mass index of participants were 33.2 years (range, 30–36), 171.7 cm (range,

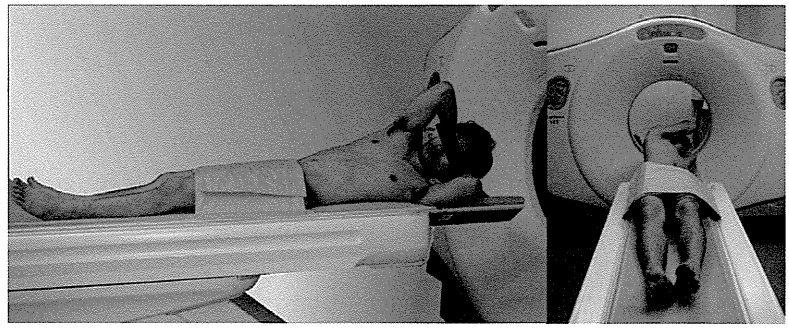

Figure 1. Acquisition of computed tomography. Subjects were instructed to perform maximum trunk rotation with the pelvis being fixed to the table. The arms were held behind their heads and the head was kept in the neutral position during rotation.

168–186), 70.5 kg (range, 57–91), and 23.9 (range, 20.2–30.4), respectively.

Main AR

At maximum rotation, mean ROM (± SD) of T1 with respect to L1 at 1 side was 24.9° ± 4.9° for AR, 7.6° ± 6.0° for coupled LB in the same direction as AR, and 1.8° ± 12.4° for coupled flexion.

At maximum rotation, mean ROM (± SD) of each vertebra with respect to the inferior adjacent vertebra to 1 side was 1.2° ± 0.8° at T1–T2, 1.6° ± 0.7° at T2–T3, 1.4° ± 0.9° at T3–T4, 1.6° ± 0.8° at T4–T5, 1.8° ± 0.7° at T5–T6, 1.9° ± 0.6° at T6–T7, 2.3° ± 0.7° at T7–T8, 2.5° ± 0.8° at T8–T9, 2.7° ± 0.6° at T9–T10, 2.6° ± 0.8° at T10–T11, 1.3° ± 0.7° at T11–T12, and 0.5° ± 0.4° at T12–L1 (Table 1). AR was significantly larger at middle segments (T6–T11) than at upper segments (T1–T6) and at lower segments (T11–L1) ($P < 0.01$) (Figure 3).

Coupled LB

Coupled LB with AR was observed predominantly in the same direction as AR except at T12–L1 (Figure 4). Mean ROM of coupled LB ranged from −0.1° to 2.0° (Table 1). Among subjects, the frequency of coupled LB to the same direction as AR was 92% at T1–T2, 96% at T2–T3, 92% at T3–T4, 88% at T4–T5, 88% at T5–T6, 85% at T6–T7, 85% at T7–T8, 54% at T8–T9, 54% at T9–T10, 73% at T10–T11, 65% at T11–T12, and 38% at T12–L1. There was no significant difference in the frequency of coupled LB in the same direction among subjects ($P = 0.3$).

Coupled Flexion-Extension

Coupled flexion-extension with AR was slight flexion within range of SD (Table 1).

Coupled Translation

Coupled translations were scarcely observed in lateral, anteroposterior, and superoinferior translation (Table 1).

DISCUSSION

To the best of our knowledge, this is the first *in vivo* study to measure 3D kinematics of each consecutive segment of the thoracic spine. Some *in vivo* biomechanical studies of the thoracic spine were performed in 2D methods using fluoroscopy. However, 2D analysis of spinal motions was not suitable for measurement of rotation and coupled motion, because of limitations such as potential magnification of errors, projection of translations as rotations, and masking by the shoulder girdles shadows.[15]

The current study demonstrated that AR of the thoracic spine ranged from 0.5° to 2.7° in trunk rotation. These values generally corresponded to previous studies (Table 2). Gregersen and Lucas[10] examined *in vivo* AR of random thoracic segments of 7 medical students by inserting Steinmann pins into the spinous processes. Although their results of segmental rotations were pieced by different subjects' data, total relative angle of T1 with respect to L1 was 42° and average segmental rotation divided by the number of mobile segments was 3.5°. Panjabi *et al*[4] reported that there was 1.5° to 2° of rotation in the thoracic spine by loading 5 Nm torque in 5 cadavers' study. Oxland *et al*[3] reported that rotation was 1.8° ± 0.7° at T11–T12 and 1.2° ± 0.7° at T12–L1 by loading 7.5 Nm of torque. Watkins *et al*[16] reported that total AR of T1 relative to T12 was 23.0° with intact rib cage and sternum, and their results corresponded to ours. During the *in vivo* study using a 3-space track system, Willems *et al*[7] reported rotation of the tripartite thoracic spine. The relative rotations of T1–T4, T4–T8, and T8–T12 were 13.6° ± 4.8°, 23.3° ± 5.9°, and 9.1° ± 5.2°, respectively, and thus the average segmental AR was approximately 4.5° from

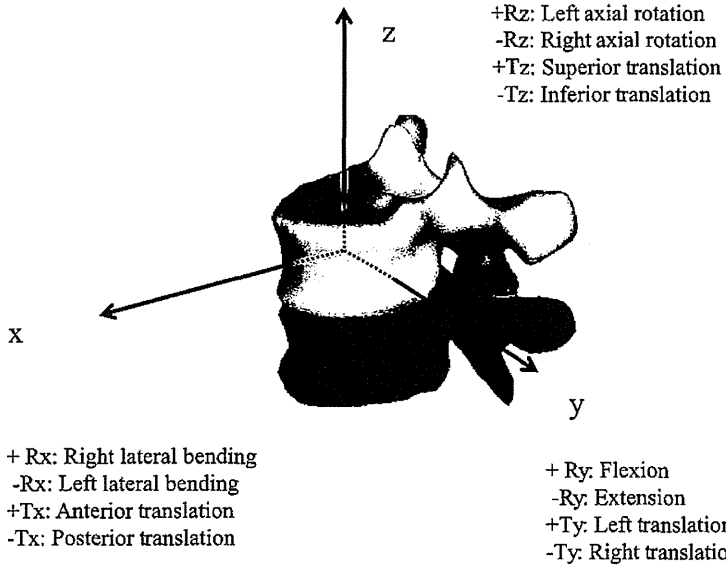

Figure 2. Orthogonal coordinate system. The origin is at the centroid of the vertebral body that is defined as half way between the centers of the 2 endplates. The local *z* axis passes through 2 centers of the endplates with upper being positive. The *y* axis is parallel to a line joining similar landmarks on the bases of the right and left pedicles with left being positive. The *x* axis is defined as perpendicular to *z* axis and *y* axis.